IEEE Access
Multidisciplinary | Rapid Review | Open Access Journal

Received 7 July 2024, accepted 18 July 2024, date of publication 22 July 2024, date of current version 1 August 2024.

Digital Object Identifier 10.1109/ACCESS.2024.3432450

RESEARCH ARTICLE

A Neural Network-Empowered Inverse FSS Design and Synthesis Approach for 5G Shielding Applications

HANEN SHALL[1], (Member, IEEE), HIBA HAWESS[2], SAHBI BACCAR[3], (Member, IEEE), AND MONCEF KADI[3]

[1]College of Engineering and Technology, American University of the Middle East, Egaila 54200, Kuwait
[2]Higher Institute of Information Technologies and Communication, University of Carthage, Borj Cedria Technopark, Carthage 1054, Tunisia
[3]ESIGELEC/IRSEEM, Université Rouen Normandie, 76000 Rouen, France

Corresponding author: Hanen Shall (hanen.shall@aum.edu.kw)

ABSTRACT In this paper, an intelligent technique for Frequency Selective Surfaces (FSS) synthesis for 5G shielding applications is presented. Our approach applies a Neural Network (NN) architecture trained on a dataset of FSS electromagnetic (EM) responses to directly predict the optimal geometrical configurations from the desired shielding specifications. The proposed solution is a very useful tool for offering radiofrequency (RF) designers a smart service to optimize RF system design considering the harmful EM environment of the device under test. The developed solution is mainly based on multivalued inverse machine learning (MIML) method. It was optimized so that it takes account of the effect of polarization and incidence angles of incident EM waves and makes the proper arrangement of the shielding FSS screen, relying on the desired frequency behavior. We demonstrate the efficiency of our proposed approach through comprehensive simulations and experimental validations. Results indicate that the proposed NN-empowered inverse FSS design proposed method achieves superior performance in terms of shielding effectiveness (SE) and design efficiency compared to traditional direct machine learning (ML) modeling approaches.

INDEX TERMS FSS, 5G, EMI, shielding, ML, intelligent, EM simulation, inverse problem.

I. INTRODUCTION

The rapid growth of wireless communication allows faster data transfer, expanded information, and increased capacity exchange channels through the enlargement of the working frequency spectrum. Simultaneously, the surrounding parasitic EM environment, that is. EM radiation and interference, becomes significantly more restrictive owing to newly designed antenna properties, increased power levels, and the integration and cohabitation of diverse electronic components [1]. Moreover, due to the allocation of new frequency bands mainly for the latest mobile networks including the fifth generation (5G) [2], [3], [4] and from now on the sixth generation (6G), the risk of frequency bandwidth intrusion with other existing wireless RF setups becomes noteworthy. Consequently, a great attention needs to be pitched to ensure electromagnetic compatibility (EMC) of latest developed RF systems. EM shielding techniques are widely used to solve such issues by isolating the victim RF components from the surrounding harsh EM environment. 5G base stations operating at 3.5 GHz band, designated as a primary band for 5G NR (New Radio) across Europe [5], can potentially interfere with systems that use nearby frequencies within the same spectrum range [6]. This electromagnetic interference (EMI) could give rise to total system dysfunction and in many cases to hazardous accidents. Not long ago, a large debate has been opened when detecting an EMI between 5G signals from airports neighboring base stations and radar altimetric embedded in aircraft systems [7].

Frequency selective surfaces (FSS) have been introduced nowadays as great candidates for EM shielding in diverse frequency bandwidths particularly in the 5G frequency range [8], [9]. Research has been focused on such structures to achieve a good SE. These RF forms are made up of metal

The associate editor coordinating the review of this manuscript and approving it for publication was Valerio De Santis.

patches or aperture arrays/units and have 2D or 3D periodic layouts.

An FSS structure can reflect or transmit incident EM waves in a specific frequency band. As a result, an electromagnetic wave filter function can be performed by introducing such geometries. The shape of the planar array elements, their periodicity, relative permittivity and thickness of the dielectric substrate, the incident wave polarization and incidence angle, all define the FSS frequency behavior.

Along with EM shielding, many other applications related to the use of FSS have been proposed. In fact, FSS based composite absorbing materials have been extensively employed in hybrid radomes [10] to decrease the target's radar cross section (RCS) [11] and produce stealth effect [12]. Moreover, to maximize the antenna's usage in parabolic antennas with sub-reflectors, FSSs have been widely employed in the construction of polarization mode converters and composite multifrequency antennas [13]. Last but not least, FSSs are frequently used in the design of multi-frequency multiplexers in satellite communication [14].

It is worth noting that these surfaces structures, which could be produced on a substrate using printed circuit board (PCB) technology, can operate as spatial filters with appropriate filtering properties. So, as one of the challenges for FSS design, microwave researchers constantly aim to find the best design technique that can effectively synthetize these structures.

The usage of computational numerical tools to simulate FSS EM characteristics with their specific geometrical parameters and properties has increased with the progress of computing resources [15]. However, the evaluation of only one single response may require a lot of computing time (hours, days, or even weeks) and supplies especially when trying to test different use cases and configurations. The growing need for more precision and the continual rise in the complexity of these structures lead to more and more time-consuming simulation processes. Moreover, these numerical methods provide the frequency response based on fixed geometrical parameters and cannot be used as synthesis methods.

The machine learning (ML) can be of a great interest in this research area. In fact, ML techniques may be successfully applied to enable the network to learn from previous experiences while enhancing performance. Big data analytics, in particular, can advance network management through the study of data that has been already created by the network. This approach is very interesting to help us design FSS arrays.

The ANN (Artificial Neural Network), a branch of ML, is capable of learning the nonlinear correlations between the physical/geometrical and electric parameters and hence the behavior of microwave devices [16]. Two ML learning approaches can be found in the literature: The forward [17], [18] and the inverse model [19], [20]. For the forward ANN model, the inputs are usually the FSS geometrical or/and physical parameters (units' size and spacing, dielectric properties, etc.,) and the outputs are the electrical parameters translating the frequency response (resonant frequency, bandwidth, transmission, and reflection coefficients, etc.,). This model can be trained to simulate the original microwave device problem, as classically done by EM simulation tools.

Many researchers have been particularly focused on these ANN forward models to put back numerical simulations drawbacks in terms of required time and computing resources [21].

However, when it comes to a structure design according to some predefined electrical requirements, considering the ANN ''inverse model'' seems to be the best solution for this purpose. In fact, to synthetize these RF structures, i.e. obtain geometrical and/or physical parameters from some desired electrical specifications, which is known as the inverse model, information is frequently processed in the opposite direction. In other words, the inputs will be electrical parameters and outputs becomes the geometrical ones. Optimization techniques along with inverse modeling methods are typically the two approaches used to tackle inverse problems. These techniques are very interesting and challenging at the same time. In fact, problems of non-uniqueness solution could be encountered in such inverse modeling procedures and the challenges here are focused towards developing approaches that could face these issues and quickly converge to the desired solution [22], [23].

In this paper, we have mainly focused on ANN inverse model to synthesize FSS structures that can be used as an EMI shielding screen to protect against 5G surrounding signals. Along with the geometrical parameters to be determined, a big focus, has been oriented towards polarization and incidence angles, which is a new contribution compared to other related research found in the literatures [24], [25], and [26]. Indeed, FSS structures are very sensitive to the incident wave angles which can affect the overall frequency behavior [27]. An efficient intelligent method has been proposed and obtained results highlight the importance of such technique to find the best shielding FSS geometry and orientation under specific operating conditions (frequency, bandwidth and shielding effectiveness).

II. FSS STRUCTURE UNDER TEST

There are mainly three frequency bands in 5G: low, medium and high. In our case, we focus mainly on the design of an FSS structure working as a band stop filter, means shielding structure around the 3.5 GHz frequency band: the 5G commercialized bandwidth [5]. As illustrated in [28], FSS structures can be classified into 4 groups as presented in Figure 1, depending on the periodic element of the structure. The first category consists of FSSs with their centers connected, such as three-legged elements Jerusalem cross, four legged elements and square spiral elements. The second category consists of loop FSSs, which include loaded three and four legged parts as well as hexagonal, circular, and square rings. Patch FSSs, like square, circular, and hexagonal

patches, are elements of the third group. The last group is a combination of the other groups. In general, the first and second groups are used for shielding applications because of the FSS reflection behavior, and the third type is mainly implemented with antenna structures to improve their performances, due to the absorption of the EM incoming waves.

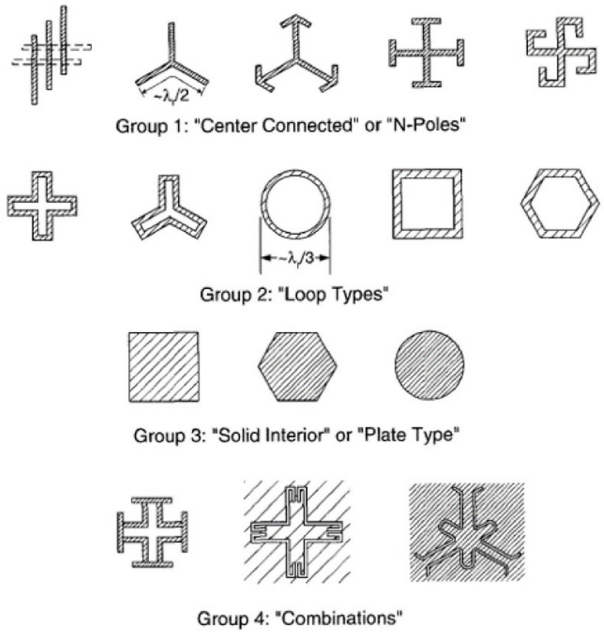

FIGURE 1. FSS different groups [28].

For illustration purposes, we have chosen a simple FSS structure from the second group (loop types): the circular loop. It is a single-turn resonant loop with a λ/3 outer diameter. This geometry can be used for shielding applications as it presents a minimum transmission coefficient at the central resonant frequency: 3.5 GHz.

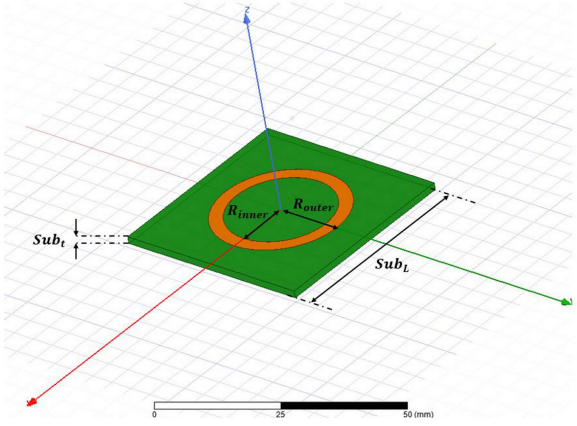

FIGURE 2. 3D view of the FSS unit cell under HFSS.

Under these resonance conditions, the FSS can be designed on an FR4 substrate with a relative dielectric constant of 4.4, a thickness of 1.6 mm and a loss tangent of 0.02. The unit cell has a square dimension of 44 mm. Hence, simulation accurately reflects the real environment of the FSS and includes comprehensive consideration of dielectric and conductive losses.

Figure 2 depicts the proposed FSS unit cell geometry. All the fixed dimensions are summarized in table 1. Accurately, R_{inner}, R_{outer}, Sub_L and Sub_t are the main parameters related to structure geometry. However, *Phi*(ϕ) and *Theta* (θ) are defined respectively as polarization and incidence angles. They are related to the incident EM wave that illuminates the structure under test. Figure 3 shows the field vector (H) that points toward the x axis, and an electric field vector (E) that points in the direction of the y axis. The incidence angle is noted θ, while the polarization angle is represented by ϕ. These angles can affect the FSS frequency characteristics and researchers are working to design novel structures insensitive to such incidence and polarization orientations [29].

Initially, the proposed FSS unit cell has been modeled and simulated using the electromagnetic simulator tool HFSS-ANSYS [30]. For the purpose to configure the simulation setup, we have fixed all the used materials, the excitation as well as the boundaries conditions.

TABLE 1. Geometrical parameters of the FSS structure.

Parameters	Description	Value
R_{inner}	Inner circle's radius	11.7 mm
R_{outer}	Outer circle's radius	14.7 mm
Phi ϕ	Polarization angle	0 degree
Theta θ	Incidence angle	0 degree
Sub_L	Substrate dimension	44 mm
Sub_t	Substrate thickness	1.6 mm

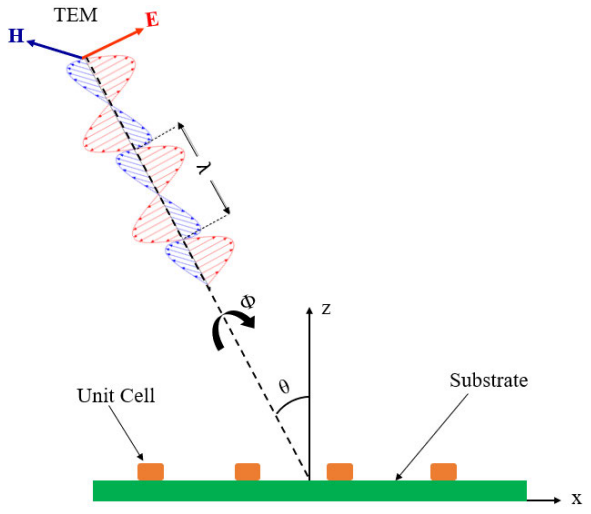

FIGURE 3. Polarization and incidence angles.

Two Floquet ports (port 1 and port 2) are used to excite plane waves under TE (Transverse Electric) and TM (Transverse Magnetic) polarization modes when placed at an

arbitrary distance below and above the FSS unit cell. Port 1 is placed above the top surface of the FSS structure. This port simulates the excitation of incident waves from the top. Port 2 is placed below the bottom surface of the FSS structure to analyze the transmission or reflection of waves through the structure.

Primary and secondary boundaries are used as limit conditions. In fact, they are frequently employed to simulate frequency selective surfaces or infinite antenna arrays.

In the context of RF applications, the reflection coefficient (S_{11}) quantifies the portion of the incident wave at port 1 that is reflected back into the same port, whereas the transmission coefficient (S_{21}) quantifies the signal transmission efficiency from port 1 to port 2 of the network under test. S_{21} for an FSS is a crucial parameter that describes how well electromagnetic waves pass through the structure from one side to the other side

For shielding applications, which is our targeted use here, the FSS screen should provide electromagnetic shielding by selectively blocking certain frequencies. Consequently, S_{21} should be minimal and S_{11} is maximal at the desired resonant (3.5 GHz).

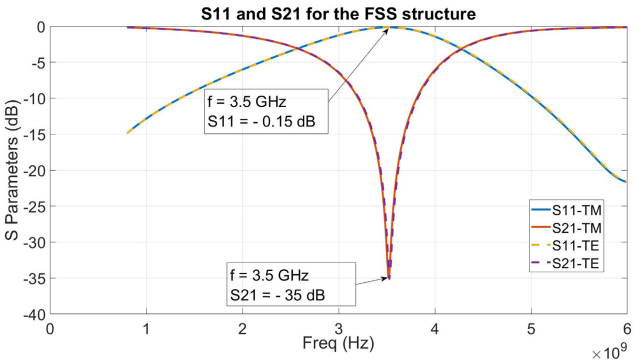

FIGURE 4. Scattering parameters for TE and TM modes under normal incidence.

S_{11} and S_{21} curves for TE and TM modes, presented in Figure 4, demonstrate that the design and analysis of the FSS-based shielding structure are successful. The 3.5 GHz frequency band is shielded using the selected FSS shape whose geometrical key-parameters are presented in Table 1. Results indicate that the shielding structure is built with a good stopband feature, as illustrated in the same figure.

To better describe the desired FSS shield, we have selected three main specifications, namely resonant frequency, bandwidth at −20 dB and the minimum level of S_{21}.

TABLE 2. Simulation results according to structure specifications.

Parameters	Description	Value
f_r	Resonant frequency	3.5 GHz
BW	Bandwidth	0.192 GHz
S_{21min}	Minimum level of S_{21}	-35,18 dB

The S_{21} minimum level ($S_{21\text{min}}$) is an indicator of the shielding effectiveness (SE). This quantity is very important to judge the shielding properties of structures under test.

Accurately, SE (in dB) is defined, according to equation 1, as the difference between the transmission characteristics with and without the Shield [31].

$$SE\ (dB) = S_{21-without\ FSS}\ (dB) - S_{21-with\ FSS}\ (dB) \quad (1)$$

where, $S_{21-\text{withoutFSS}}$ (dB) is a transmission parameter without the shield and $S_{21-\text{withFSS}}$ (dB) is the transmission parameter with shield. The same simulation has been performed without the presence of the FSS unit cell to quantify the SE for the structure under test.

III. IMPLEMENTATION OF THE PROPOSED TECHNIQUE

The main purpose of our work is to develop an intelligent technique based on artificial neural network (ANN) to solve the inverse problem in FSS structure design. This inverse problem involves determining the FSS's geometrical parameters that will produce the desired frequency or electrical response. Unlike other classical approaches presented in the literatures [19] and [20], our proposed modeling methodology takes account of the polarization and incidence angles along with the geometrical parameters to predict later an optimized FSS structure arrangement for shielding purposes in the real environment. To achieve the desired target, different steps have been carried out as presented in Figure 5:

(i) Step1: Data Collection
(ii) Step 2: Data preparation
(iii) Step 3: NN inverse technique implementation
(iv) Step 4: Results validation

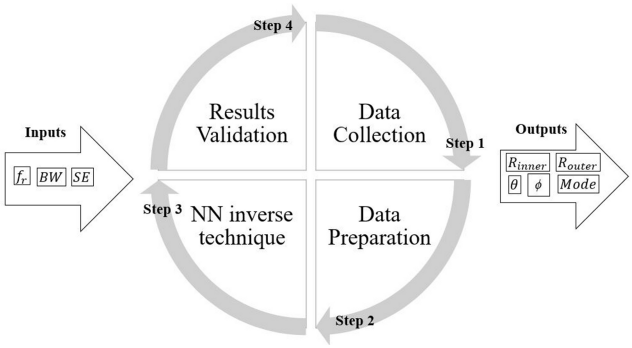

FIGURE 5. Overview of the different steps for the proposed technique.

A. DATA COLLECTION AND PREPARATION

In order to build up our proposed technique, we need to prepare dataset for the training phase. This step is very important because the model will learn based on this created dataset. This data typically consists of input-output pairs, where the inputs are the desired FSS frequency behavior (f_r, BW, SE), and the outputs are the geometric design and recommended orientations (R_{inner}, R_{outer}, $Mode$, θ and ϕ).

As aforementioned, research prove that the frequency response of FSS structures depends on both the incident

and polarization angles. Consequently, these parameters are considered for this study along with the geometrical characteristics and the polarization modes (TE and TM), contrary to other traditional approaches that omit the angles effects. The FSS response should be analyzed based on this input-output association. To accomplish this task, we have carried out different EM simulations under ANSYS-HFSS [30], to get the required database from scratch.

For this work, we rely on the FSS structure geometry presented in section II. Based on this selected model and being delimited by the unit cell substrate dimensions, different parametric simulations have been carried out with varying parameters to collect data for training and obtain the initial dataset. Four variables have been tuned including geometrical parameters along with incidence and polarization angles, for both TE and TM modes; these simulations allowed us to systematically vary FSS geometries (R_{inner} and R_{outer}) and observe their frequency behaviors under controlled conditions (polarization angle, incidence angle and polarization mode).

For our simulations, we varied key geometric parameters of the FSS structure based on the available substrate space taken as illustrative example; we varied R_{inner} from 2 mm to 11 mm, R_{outer} from 12 mm to 21.5 mm with a step of 0.5 mm for both parameters. Moreover, incidence and polarization angles have been tuned; we examined a range of angles, typically from normal incidence (0 deg) to oblique angles up to 80 deg.

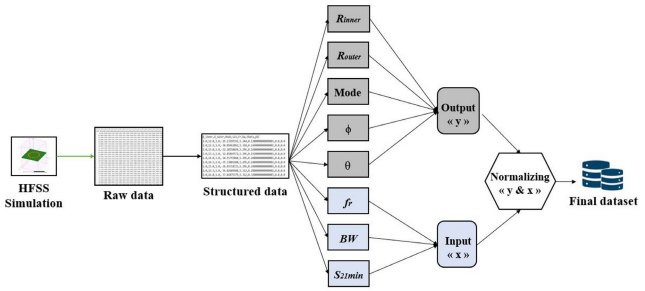

FIGURE 6. Data preparing for the proposed inverse model.

During the simulation campaigns, we collected data points for the reflection and transmission coefficients across various frequencies up to 8 GHz for each geometrical configuration. These data were named ''Raw data'' as presented in Figure 6.

While proceeding, we divided our simulation campaigns into distinct phases. Each phase, taking around 12 hours, focused on a specific aspect or combination of parameters to ensure a thorough and organized analysis

After obtaining these data in a form of distinct frequency-geometry pairs, the next step is to organize them into a structured format called ''Structured data'' where each entry corresponds to a specific geometrical/simulation configuration (R_{inner}, R_{outer}, $Mode$, θ and ϕ) and its associated frequency response (f_r, BW, SE).

The step-by-step process to prepare the parameters data, from this initial exploded and unstructured data, is depicted in Figure 6.

Based on the defined input-output in Figure 5, data preprocessing steps have been implemented to prepare structured dataset in a suitable format for training the ML model, so that, 8726 distinct input-output pairs have been collected.

After identifying our input and output presented by ''x'' and ''y'' respectively, a data normalization should be carried out to finish the last step for the data collection and preparation.

B. ANN-BASED INVERSE TECHNIQUE

In the context of RF structure design or even other engineering problems, the inverse modeling approach can be used as reverse engineering procedure used for decision-making process for a particular design or optimization process. It is based on specifying the objective or performance metric that designers want to optimize to get the resulting RF geometry. In other words, the inverse modeling approach is used to predict the geometry from the desired frequency response that results from. This is mainly the goal of our approach for the synthesis of FSS structures which can be employed as a shield for 5G applications.

These modeling approaches are very promising since they help RF designers to predict desired RF geometries, based on some desired specifications, without performing intensive numerical simulations which is really the case for FSS structures.

For such modeling procedure, the challenge is to find an optimized solution to the non-uniqueness problem [32], [33]. Indeed, multiple solutions can fit the observed data equally well. This non-uniqueness problem poses significant challenges in interpreting and resolving the inverse problem. To overcome this problem, our proposed solution has been inspired from the presented approach in [23] and updated to fit our modeling objectives. In one hand, the proposed technique is easy to implement, in another hand, it does not need neither huge mathematical expressions nor a complex structure for the neural network perceptron. The description of the proposed model is illustrated in Figure 7. A single set of electrical parameters with many sets of geometrical characteristics is considered by using a multivalued neural network inverse modeling technique.

Where:

- m: is the number of outputs, $m = 5$.
- n: is the number of inputs, $n = 3$.
- N: is the number of duplicated results.
- x_n: is the input vector [f_r, BW, SE].
- $y_{m,i}$: is the output vector from the proposed model [R_{inner}, R_{outer}, Mode, ϕ, θ], with $i = 1, 2, \ldots N$
- $F_{n,i}$: is the output vector from the forward model [f_r, BW, SE], with $i = 1, 2, \ldots N$
- E: is the error between the input vector X and the different outputs of the forward model $F_{n,i}$.

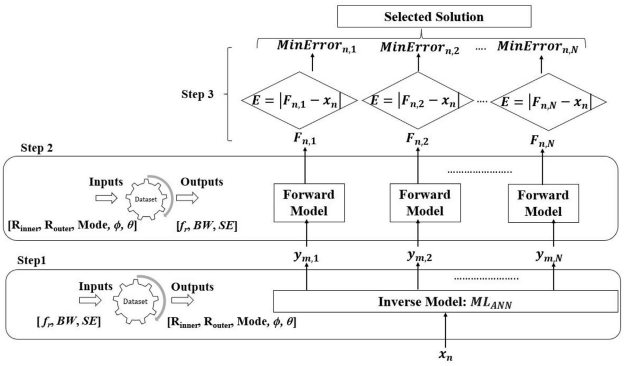

FIGURE 7. Diagram for the synthesis method.

As presented in Figure 7, the first step (step1) which is the inverse model is prepared by repeating the outputs of the direct inverse model N times as described in equation 2:

$$[y_1 y_2 \ldots\ldots y_N] = ML_{ANN}(x) \tag{2}$$

where the inverse model for a multivalued neural network is denoted by $\mathrm{ML_{ANN}}$, a multilayer perceptron (MLP) with $i = 1, 2, \ldots,$N, $\mathrm{y_i}$ is the $\mathrm{i^{th}}$ value of the suggested inverse model for input x_n. Each value y_i is an m-vector containing all the geometrical parameters.

These obtained outputs y_i with $\mathrm{i} = 1, 2,\ldots N$, are then processed through a forward (direct) MLP model (step 2) to find out corresponding geometrical parameters, $\mathrm{F_{n,i}}$ with $\mathrm{i} = 1, 2,\ldots N$. Actually, inverse model inputs are frequency responses [f_r, BW, SE], while the outputs are geometrical/operational parameters [$\mathrm{R_{inner}}$, $\mathrm{R_{outer}}$, Mode, ϕ, θ], whereas those of the forward model are typically the opposite. Figure 7 illustrates how each model operates.

For the inverse modeling approach, we have used three input neurons employing "ReLu" activity function and three hidden layers. For the first hidden layer, there are 30 neurons with "tanh" activity function. For the second layer, there are 30 neurons with the same activation function. Finally, for the third one, we fixed the number of neurons to 15 and $m \times N$ neurons for the output layer. The MLP is described as a 3-30-30-15-5 $\times N$ neurons structure. These parameters have been chosen after carrying out several tests to optimize the error function. Table 3 displays the result of the training phase according to the custom error function described in equation 3 [23].

$$E = \sum_{k \in T_r} E_k \tag{3}$$

where $\mathrm{T_r}$ is the index set of all the training samples and $\mathrm{E_k}$ is the training error for the $\mathrm{k^{th}}$ training sample which is described in equation 4 as follows:

$$E_k = \left(\sum_{i=1}^{N} \frac{1}{er_{i,k}} \right)^{-1} \tag{4}$$

where $er_{i,k}$ is defined as the error between $\mathrm{y_i}$ and $\mathrm{t_k}$ as expressed in equation 5:

$$e_{i,k} = \frac{1}{2} \| y_i - t_k \|^2 \tag{5}$$

where y_i is the $\mathrm{i^{th}}$ value of the inverse model $\mathrm{ML_{ANN}}$ for the input x_k and t_k is the $\mathrm{k^{th}}$ output training sample.

TABLE 3. Test error result for the inverse model.

Parameters	Loss Function
R_{inner}	3.17e-06
R_{outer}	2.20e-06
θ	1.67e-06
ϕ	1.35e-07
Mode	4.48e-07

For the forward modeling approach, we have used five input neurons using "ReLu" activity function and three hidden layers. For the first hidden layer, there are 30 neurons with "tanh" activity function. For the second one, there are 30 neurons with the same activation function. Finally, for the third hidden layer, we fixed the number of neurons to 15 and three neurons for output layer. The forward neural network (FNN) is described as a 5-30-30-15-3 neurons structure.

For our multivalued algorithm, our challenge is to choose the optimal value of N, that means how much we should duplicate our output. Some tests have been carried out for this purpose. We can conclude that the bigger N is, the more the error drops, thus we ultimately decided on $N = 3000$ but with an epoch number equal to 5. In fact, it is a sort of trade-off between the model precision, the computing hardware resources and the required training time. The choice of 3000 is decided based on approximated duplicated electrical parameters found in the final dataset. For the aforementioned conditions ($N = 3000$, epoch number $= 5$), the loss function was quantified to be 2.2e-06.

Figure 8 compares different samples (sample1, sample2 and sample3) for both the transmission and reflection coefficients. Green curves are the desired $\mathrm{S_{21}}$ and $\mathrm{S_{11}}$ whereas blue curves represent EM simulation results of the synthetized FSS design. A very good agreement can be highlighted.

Now, we proceed to compare our obtained results with classical modeling approaches. We have chosen to compare the scattering parameters with the classical direct ML approach, in which the non-uniqueness problem is not treated. For this traditional (classical) ML approach, we apply inputs [f_r, BW, SE] to the MLP without any duplication. The output is the set of geometrical/operational parameters [$\mathrm{R_{inner}}$, $\mathrm{R_{outer}}$, Mode, ϕ, θ], as presented in Figure 9. We have considered the same MLP as the forward model.

For the classical direct approach, the non-uniqueness problem is not addressed. Indeed, multiple solutions can fit the observed data equally well. This lack of a single unique solution can cause challenges for new predictions, consequently for model generalization. Hence, using this

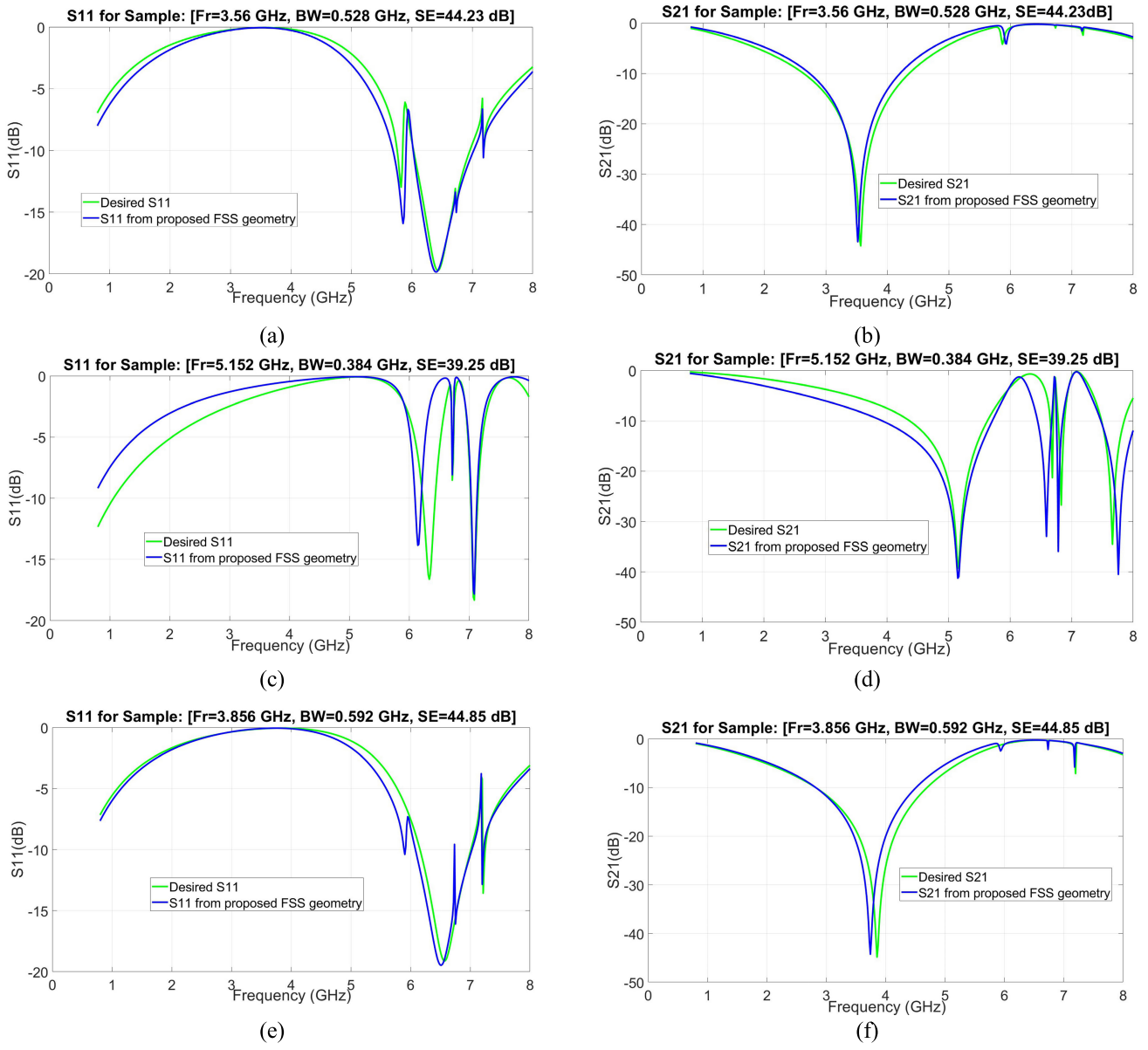

FIGURE 8. Comparison between simulated and predicted scattering parameters for 3 different samples: Sample 1 [$f_r = 3.56$ GHz, BW = 0.528 GHz and SE = 44.23 dB], Sample 2 [$f_r = 5.152$ GHz, BW = 0.384 GHz and SE = 39.255 dB], Sample 3 [$f_r = 3.856$ GHz, BW = 0.592 GHz and SE = 44.85 dB] (a) S11-Sample1 (b) S21-Sample1 (c) S11-Sample2 (d) S21-Sample2 (e) S11-Sample3 (f) S21-Sample3.

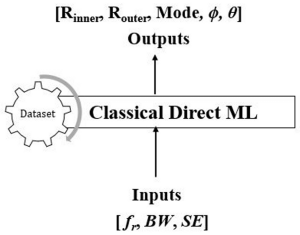

FIGURE 9. Diagram of the classical direct ML network.

method, we obtained results that diverged from the desired parameters, while our approach provided accurate results in alignment with the expectations. Figure 10 illustrates clearly the comparison results and highlights undoubtedly that the proposed solution significantly improves the results accuracy compared to the classical ML approaches.

IV. EXPERIMENTAL RESULT

In order to practically check the validity of the proposed FSS synthesis approach, a printed circuit board-based prototype was fabricated. The FSS structure, composed of 8×8 elements, consists of 44 mm $\times$ 44 mm unit cells, having an overall size of approximately 352 mm $\times$ 352 mm. The prototype was fabricated on a FR-4 substrate with a relative permittivity $\varepsilon_r = 4.4$, thickness $Sub_t = 1.6$ mm and loss tangent $tan\delta = 0.02$.

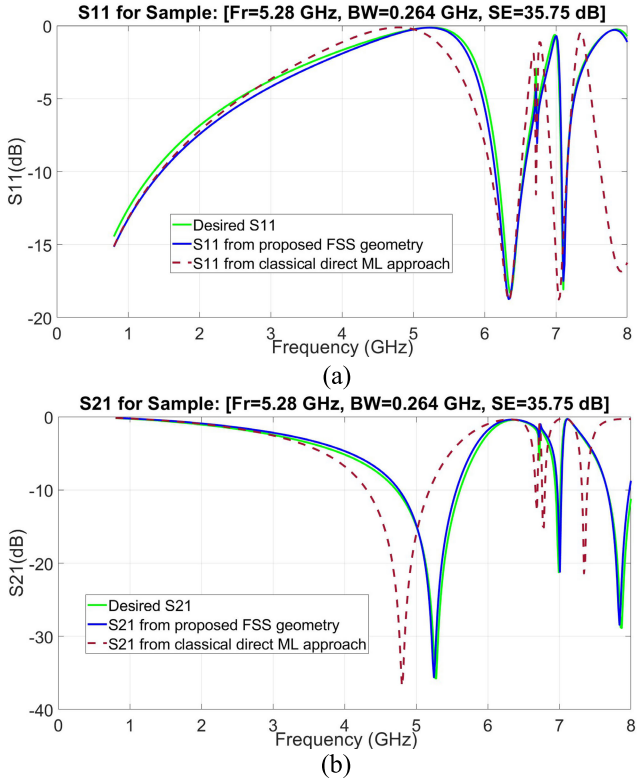

FIGURE 10. Comparison of results from traditional approaches with the proposed solution response (a) Reflection coefficients (b) Transmission coefficients.

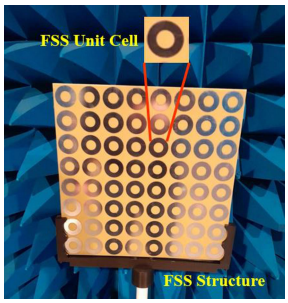

FIGURE 11. Fabricated FSS structure.

Experimental scenarios are chosen to be different from those presented in both figures 8 and 9 with a view to have more samples built on various requirements and geometries for validation purposes. Essentially, two settings have been considered as illustrative cases:

- Setting 1:

Required user inputs: [$f_r = 4.064$ GHz, $BW = 0.576$ GHz and $SE = 44.44$ dB]

Desired calculated outputs: [$R_{inner} = 9.5$ mm, $R_{outer} = 19.5$ mm, Mode = TM, $\phi = 0$ deg, $\theta = 0$ deg]

- Setting 2:

Required user inputs: [$f_r = 3.92$ GHz, $BW = 0.384$ GHz and $SE = 44.02$ dB]

Desired calculated outputs: [$R_{inner} = 9.5$ mm, $R_{outer} = 19.5$ mm, Mode = TM, $\phi = 0$ deg, $\theta = 30$ deg]

Based on the inverse proposed methodology presented in section III and after training the model, the synthesis is obtained according to the desired criteria within 1 minute computation time.

TABLE 4. Setting 1 for experimental validation.

Output Parameters	Desired	Predicted
R_{inner}	9.5 mm	9.62 mm
R_{outer}	19.5 mm	19.57 mm
θ	0 deg	4.7 deg
ϕ	0 deg	4.9 deg
Mode	TM (Mode=2)	TM (Mode=2)

TABLE 5. Setting 2 for experimental validation.

Output Parameters	Desired	Predicted
R_{inner}	9.5 mm	9.65 mm
R_{outer}	19.5 mm	19.34 mm
θ	30 deg	32.03 deg
ϕ	0 deg	5 deg
Mode	TM (Mode=2)	TM (Mode=2)

The hardware configuration for the used computer system is 11th Gen Intel(R) Core (TM) i5-11400H @ 2.70GHz with 16 GB installed RAM memory. The obtained results are summarized in Tables 4 and 5 for both settings.

The desired and predicted outcomes harmonize perfectly with slight disparities for the angles' prediction due to the limited data points for these orientations during the dataset preparation phase. Actually, R_{inner} tuning has been adjusted from 2 mm to 11 mm in increments of 0.5 mm, R_{outer} from 12 mm to 21.5 mm in increments of 0.5 mm, whereas θ and ϕ from 0 deg to 80 deg in increments of 10 deg, which corresponds to less observations for these angles' attributes. These tuning adjustments have been refined due to memory constraints caused by computational resource limitations.

According to the predicted geometrical parameters, FSS structure has been fabricated as showcased in Figure 10. The measurement has been carried out using the free-space method in a microwave anechoic chamber to eliminate potential unwanted interferences caused by the external environment. A pair of double ridge horn antennas having a frequency range from 700 MHz to 18 GHz, positioned at 1m far from the structure under test, have been used for our measurement setup as illustrated in Figure 11.

The polarization and incidence angles have been experimentally used to make the proper orientation of the FSS structure with respect to the incident wave, taking into account the non-negligible effect of these aforementioned angles, in contrast to other pervious research works. In other words, for real shielding applications and in order to reach the desired frequency response, FSS structure orientation vs the incident wave can be adjusted according to the predicted

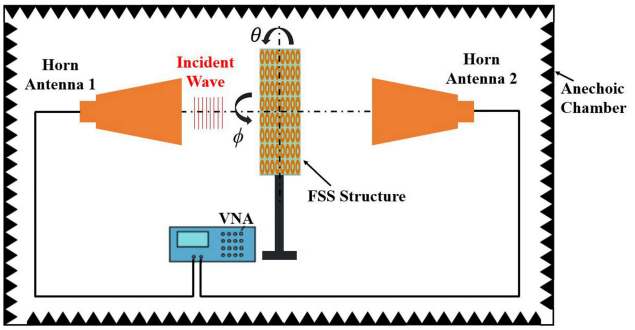

(a)

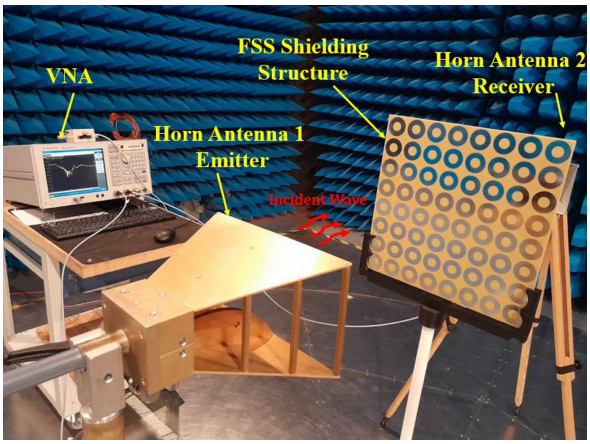

(b)

FIGURE 12. (a) Schematic diagram of the measurement setup (b) Photo of the measurement setup in a microwave anechoic chamber.

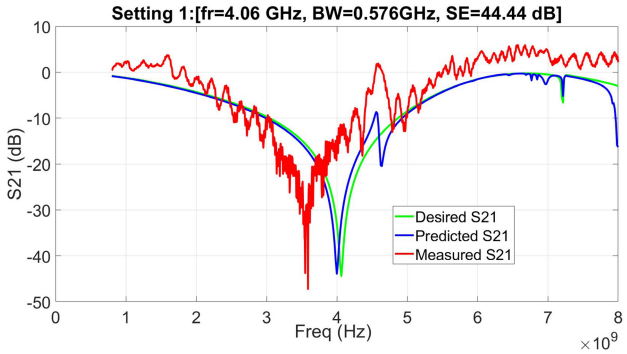

(a)

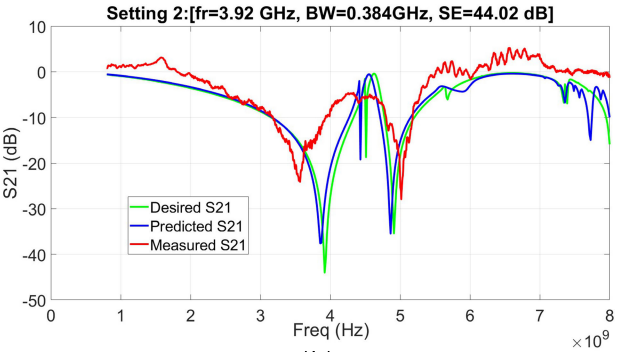

(b)

FIGURE 13. Predicted, desired and measured transmissions coefficients for the FSS structure under test for different scenarios (a) Setting 1, (b)Setting 2.

angles θ and ϕ which will make the shielding design more efficient towards incoming EMI. Experimental results were obtained using an Agilent Technologies E5071C vector network analyzer (VNA). The measurement setup diagram and photo are presented in Figure 12.

As ascertained in both tables 4 and 5, TM polarization was assumed for our measurement drives. The measured, simulated and predicted transmission coefficients depicted in Figure 13.

As expected, the results presented in both tables 4 and 5 as well as figure 13 demonstrate a very strong correlation between prediction and simulation. Moreover, the measurement procedures reveal a harmonious relationship between measured, desired, and predicted transmission coefficients. Slight difference may be observed mainly for the measured data, which can be attributed to several factors related to the measurement environment, setup and manual procedure. In fact, the placement of the FSS structure holder with respect to both emitter and transmitter horn antennas is non-automatically operated, which can introduce potential measurement errors mainly in setting 2. In fact, for this setting, the shielding structure has been positioned with an angle of 30 degree with respect to the incident wave. This manual positioning introduces a slight shift in the resonant frequency related the holder's orientation angles and positioning, affecting the measurements accuracy.

Furthermore, manual procedure introduces also misalignments between the two horn antennas which can affect results. Additionally, when conducting measurements in a semi-anechoic chamber rather than a fully anechoic chamber, certain errors can be introduced due to the differences in their electromagnetic surrounding environment. However, obtained results are very encouraging and enables us to successfully validate our neural network-empowered inverse FSS Design approach.

V. CONCLUSION

In this paper, we have presented a novel method for the synthesis of FSS design for 5G EM shielding applications, around the 3.5GHz frequency range. The adopted FSS unit cell is a circular conductive ring printed on an FR4 substrate and infinitely duplicated in a periodic arrangement in order to put in place a shielding screen against harmful 5G waves. An inverse ML-based solution has been implemented to take electric characteristics conditions (f_r, BW and SE) as inputs for shielding basis and proposes adequate outputs in terms of geometrical parameters and structure arrangement with respect to incident EM wave (R_{inner}, R_{outer}, $Mode$, θ and ϕ). Contrary to other synthesis approaches, our modeling method takes into account the incidence and polarization angles of the incident wave due to their significant effects on the FSS frequency response.

The suggested method combines the inverse and direct neural networks to choose the valid solution from N different numerous sets of geometrical parameters linked to a single set of electrical specifications to overcome the problem of non-uniqueness solution and provide high- quality results. For validation intent, different samples have been considered. The good agreement between predicted, simulated and measured results enables us to successfully validate the proposed approach and make it more efficient compared to other traditional ML approaches or numerical computation methods.

In conclusion, we discuss the prospects of developing a fully automatic setup within a fully anechoic chamber to enhance measurement accuracy. Moreover, the proposed technique can be extended to cover the 6G band by preparing constructed dataset for this frequency range. Furthermore, the proposed approach can be used to synthetize more complex structures with different materials, substate layers using more complex unit cells geometrical forms. For this purpose, the modeling approach needs to optimize more parameters based on required frequency behavior to cover further use cases for shielding purposes.

ACKNOWLEDGMENT

The authors would like to thank IRSEEM-ESIGELEC Laboratory Team, France, for providing the measurement platform to perform all the characterization steps for the experimental validation of their proposed approach.

REFERENCES

[1] P. F. Wilson, K. A. Remley, W. F. Young, C. A. Gentile, J. M. Ladbury, and D. F. Williams, "A NIST perspective on metrology and EMC challenges for 5G and beyond," *IEEE Electromagn. Compat. Mag.*, vol. 7, no. 4, pp. 77–85, Apr. 2018, doi: 10.1109/MEMC.2018.8637299.

[2] A. Osseiran, J. F. Monserrat, and P. Marsch, *5G Mobile and Wireless Communications Technology*. Cambridge, U.K.: Cambridge Univ. Press, 2016.

[3] J. Rodriguez, *Fundamentals of 5G Mobile Networks*. Hoboken, NJ, USA: Wiley, 2015.

[4] M. Attaran and S. Attaran, "Digital transformation and economic contributions of 5G networks," *Int. J. Enterprise Inf. Syst.*, vol. 16, no. 4, pp. 58–79, Oct. 2020.

[5] *On Amending Decision 2008/411/EC As Regards an Update of Relevant Technical Conditions Applicable to the 3 400–3 800 MHz Frequency Band*, document 2019/235, Commission Implementing Decis. (EU), Jan. 2019.

[6] D. Qi, X. Xi, C. Zhang, B. Tang, and X. Liu, "Electromagnetic interference from 5G base station antenna in substation on secondary equipment," in *Proc. IEEE 2nd China Int. Youth Conf. Electr. Eng. (CIYCEE)*, Chengdu, China, Dec. 2021, pp. 1–7.

[7] *Assessment of C-Band Mobile Telecommunications Interference Impact on Low Range Radar Altimeter Operations*, document 274-20/PMC-2073, SC-239, RTCA, Inc. Program, Oct. 2020.

[8] D. Li, T.-W. Li, E.-P. Li, and Y.-J. Zhang, "A 2.5-D angularly stable frequency selective surface using via-based structure for 5G EMI shielding," *IEEE Trans. Electromagn. Compat.*, vol. 60, no. 3, pp. 768–775, Jun. 2018, doi: 10.1109/TEMC.2017.2748566.

[9] Y. Li, P. Ren, and Z. Xiang, "A dual-passband frequency selective surface for 5G communication," *IEEE Antennas Wireless Propag. Lett.*, vol. 18, pp. 2597–2601, 2019, doi: 10.1109/LAWP.2019.2944936.

[10] Z. Qiang and Z. Zhipeng, "Research on RCS of FSS radome," in *Proc. IEEE Asia–Pacific Conf. Antennas Propag. (APCAP)*, Auckland, New Zealand, Aug. 2018, pp. 452–453, doi: 10.1109/APCAP.2018.8538120.

[11] H. U. Tahseen, L. Yang, and X. Zhou, "Design of FSS-antenna-radome system for airborne and ground applications," *IET Commun.*, vol. 15, no. 13, pp. 1691–1699, Apr. 2021, doi: 10.1049/cmu2.12181.

[12] H. Shin, D. Yoon, D.-Y. Na, and Y. B. Park, "Analysis of radome cross section of an aircraft equipped with a FSS radome," *IEEE Access*, vol. 10, pp. 33704–33712, 2022, doi: 10.1109/ACCESS.2022.3162262.

[13] S. Singh, V. Binzlekar, S. Jorwal, R. Panwar, and S. Agarwal, "A miniaturized, polarization and angle stable hexagonal FSS for stealth applications," in *Proc. IEEE Indian Conf. Antennas Propag. (InCAP)*, Rajasthan, India, Dec. 2021, pp. 723–726, doi: 10.1109/InCAP52216.2021.9726405.

[14] U. Jamwal, N. Narang, D. Singh, and K. L. Yadav, "Investigating the improved microwave absorption bandwidth in Fe/ZnO composite-backed cross-dipole FSS: A critical analysis," in *Proc. IEEE Wireless Antenna Microw. Symp. (WAMS)*, Jun. 2023, pp. 1–5, doi: 10.1109/WAMS57261.2023.10242883.

[15] T.-K. Wu, "Four-band frequency selective surface with double-square-loop patch elements," *IEEE Trans. Antennas Propag.*, vol. 42, no. 12, pp. 1659–1663, Dec. 1994, doi: 10.1109/8.362804.

[16] J. Qiu, Z. Huang, Z. Zhang, and D. Tang, "Modeling method of active metasurface based on artificial neural network and microwave network," in *IEEE MTT-S Int. Microw. Symp. Dig.*, Nov. 2023, pp. 1–3, doi: 10.1109/IMWS-AMP57814.2023.10381409.

[17] P. Chawla and R. Khanna, "Design and optimization of RF MEMS switch for reconfigurable antenna using feed-forward back-propagation ANN method," in *Proc. Nirma Univ. Int. Conf. Eng. (NUiCONE)*, Ahmedabad, India, Dec. 2012, pp. 1–6, doi: 10.1109/NUICONE.2012.6493245.

[18] P. Mahouti, "Design optimization of a pattern reconfigurable microstrip antenna using differential evolution and 3D EM simulation-based neural network model," *Int. J. RF Microw. Comput.-Aided Eng.*, vol. 29, no. 8, Apr. 2019, Art. no. e21796, doi: 10.1002/mmce.21796.

[19] R. M. S. Cruz, P. H. da F. Silva, and A. G. D'Assuncao, "Synthesis of crossed dipole frequency selective surfaces using genetic algorithms and artificial neural networks," in *Proc. Int. Joint Conf. Neural Netw.*, Atlanta, GA, USA, Jun. 2009, pp. 627–633, doi: 10.1109/IJCNN.2009.5178927.

[20] L. C. M. M. Fontoura, H. W. De Castro Lins, A. S. Bertuleza, A. G. D'assunção, and A. G. Neto, "Synthesis of multiband frequency selective surfaces using machine learning with the decision tree algorithm," *IEEE Access*, vol. 9, pp. 85785–85794, 2021, doi: 10.1109/ACCESS.2021.3086777.

[21] Y. Yang, S. Xinyang, and C. Fang, "Full connected neural networks substitute traditional electromagnetic simulations to calculate target objects' RCS," in *IEEE MTT-S Int. Microw. Symp. Dig.*, Guangzhou, China, Nov. 2022, pp. 1–3, doi: 10.1109/IMWS-AMP54652.2022.10106903.

[22] H. Lv, L.-Y. Xiao, H.-J. Hu, and Q. Huo Liu, "A spatial inverse design method (SIDM) based on machine learning for frequency-selective-surface (FSS) structures," *IEEE Trans. Antennas Propag.*, vol. 72, no. 3, pp. 2434–2444, Mar. 2024, doi: 10.1109/TAP.2024.3355227.

[23] C. Zhang, J. Jin, W. Na, Q.-J. Zhang, and M. Yu, "Multivalued neural network inverse modeling and applications to microwave filters," *IEEE Trans. Microw. Theory Techn.*, vol. 66, no. 8, pp. 3781–3797, Aug. 2018, doi: 10.1109/TMTT.2018.2841889.

[24] S. Nanda, P. K. Sahu, and R. K. Mishra, "Inverse artificial neural network modeling for metamaterial unit cell synthesis," *J. Comput. Electron.*, vol. 18, no. 4, pp. 1388–1399, Jul. 2019.

[25] L. A. Belfore, A. A. Arkadan, and B. M. Lenhardt, "ANN inverse mapping technique applied to electromagnetic design," *IEEE Trans. Magn.*, vol. 37, no. 5, pp. 3584–3587, Sep. 2001, doi: 10.1109/20.952667.

[26] J. Jin, F. Feng, W. Na, S. Yan, W. Liu, L. Zhu, and Q. Zhang, "Recent advances in neural network-based inverse modeling techniques for microwave applications," *Int. J. Numer. Modell., Electron. Netw., Devices Fields*, vol. 33, no. 6, Nov. 2020, Art. no. e2732, doi: 10.1002/jnm.2732.

[27] J. Jin, C. Zhang, F. Feng, W. Na, J. Ma, and Q.-J. Zhang, "Deep neural network technique for high-dimensional microwave modeling and applications to parameter extraction of microwave filters," *IEEE Trans. Microw. Theory Techn.*, vol. 67, no. 10, pp. 4140–4155, Oct. 2019, doi: 10.1109/TMTT.2019.2932738.

[28] B. A. Munk, *Frequency Selective Surfaces: Theory and Design*. Hoboken, NJ, USA: Wiley, 2005.

[29] M. L. Hakim, T. Alam, and M. T. Islam, "Polarization insensitive and oblique incident angle stable miniaturized conformal FSS for 28/38 GHz mm-wave band 5G EMI shielding applications," *IEEE Antennas Wireless Propag. Lett.*, vol. 22, no. 11, pp. 2644–2648, Nov. 2023, doi: 10.1109/LAWP.2023.3284860.

[30] (2013). *HFSS From Ansys*. [Online]. Available: http://www.ansys.com/Products/Simulation+Technology/Electromagnetics/Signal+Integrity+&+Power+Integrity/ANSYS+HFSS
[31] N. Shen, L. Yan, X. Zhao, and R. Xian-Ke Gao, "Electromagnetic shielding effectiveness analysis of enclosure incorporating frequency selective surface," in *Proc. Int. Symp. Electromagn. Compat. EMC Eur.*, Sep. 2020, pp. 1–4, doi: 10.1109/EMCEUROPE48519.2020.9245755.
[32] P. Savenko, "The nonuniqueness of solutions to the synthesis problems of plane array by the prescribed amplitude directivity pattern," in *Proc. 23rd Int. Seminar/Workshop Direct Inverse Problems Electromagn. Acoustic Wave Theory (DIPED)*, Tbilisi, Georgia, Sep. 2018, pp. 129–133, doi: 10.1109/DIPED.2018.8543298.
[33] N. Levashova, A. Gorbachev, R. Argun, and D. Lukyanenko, "The problem of the non-uniqueness of the solution to the inverse problem of recovering the symmetric states of a bistable medium with data on the position of an autowave front," *Symmetry*, vol. 13, no. 5, p. 860, May 2021, doi: 10.3390/sym13050860.

HANEN SHALL (Member, IEEE) received the Ph.D. degree in electronics from the University of Rouen "Haute Normandie", France, in 2014, and the degree in electrical engineering and the M.Sc.Res. degree in electronics from the Graduate School of Engineering, University of Sfax, Tunisia, in 2009 and 2010, respectively. She is currently an Assistant Professor with American University of the Middle East (AUM), Kuwait. She has more than 14 years of international experiences. Throughout her career, she worked on different national and international research projects, with academic and industrial partners, related to electromagnetic compatibility (EMC) for electronic devices/systems, innovation on microelectronics and nanotechnology for sensors, and emerging technology for IoT applications. Her research interests include design and synthesis of emergent RF components/systems and antennas technologies for IoT applications taking into account harsh EM surrounding environment and include all the steps for numerical, analytic, or AI-based modeling, EM simulation, and EMC characterization according to international standards.

HIBA HAWESS received the degree from the Higher Institute of Information Technologies and Communication (ISTIC), Tunisia, and the Research Master's degree in robotics computer science and communication systems "data science and smart services" from ISTIC, in 2022. She was mainly interested in the application of these modeling approaches for RF systems design. During her master's project, she had been focused on the design of frequency-selective surfaces for 5G electromagnetic shielding purposes based on machine learning techniques. She has been used to deploy variety of programming languages for ANN-based pattern. She is strongly interested in merging the realms of telecommunication systems and artificial intelligence for new forthcoming challenges. Her main research interests include prediction and modeling using ANN algorithms for different requests.

SAHBI BACCAR (Member, IEEE) received the National Engineer degree in telecommunications engineering and the M.S. degree in information and communication technologies from the High School of Communications of Tunis (Sup'Com), Ariana, Tunis, in 2005 and 2007, respectively, and the Ph.D. degree in electronics from the University of Bordeaux, in 2012. He was a Research and Development Electrical Engineer with the Schlumberger Riboud Product Center, Clamart, France, for 4 years. He is currently an Associate Professor of electronics with ESIGELEC and a member of IRSEEM Laboratory a joint Laboratory with the University of Rouen, Normandy, France. He has more than 15 years of experience in academia and industry in Tunisian and French companies and universities. He worked on the modeling of High Temperature Analog and Mixed-Signal Circuits. His current research interests include backscatter communications, energy harvesting, RFID systems, software defined radio, emergent RF systems and antenna technologies for 5G, beyond-5G, and the Internet of Things (IoT) applications.

MONCEF KADI received the Electr. Eng. Dipl. degree from the University of Constantine, Algeria, in 1996, the Master of Research (D.E.A) degree in optoelectronic, optics, and microwaves from the National Polytechnic Institute of Grenoble (INPG), Grenoble, France, in 2001, and the Ph.D. degree in RF and optics from the University Joseph Fourier, Grenoble, in 2004. He completed his dissertation to lead research works ("HDR: Habilitation à Diriger des Recherches") with the University of Rouen Normandie, in 2011. In October 2004, he joined Ecole Supérieure d'Ingénieurs (ESIGELEC), Rouen, France, as an Associate Professor. Since 2011, he has been the Head of the Electronic and Systems Research Group, Research Institute for Embedded Systems (IRSEEM) Laboratory. He supervised and directed 20 Ph.D. students. He has coauthored more than 100 international journal articles, international and national conference papers, and international text book chapters. He is regularly involved in national/international research projects with academic and industrial partners. His current research interests include the area of EMC (electromagnetic compatibility) modeling and characterization, thermal effect on electronic components and systems, active antennas for 5G and aeronautic applications, energy harvesting and reliability, and robustness of wide gap GaN and SiC power transistors.